Hydrodynamic Simulation of Co-Current and Counter Current of Column Distillation Using Euler Lagrange Approach

H. Troudi, M. Ghiss, Z. Tourki, M. Ellejmi

Abstract—Packed columns of liquefied petroleum gas (LPG) consists of separating the liquid mixture of propane and butane to pure gas components by the distillation phenomenon. The flow of the gas and liquid inside the columns is operated by two ways: The co-current and the counter current operation. Heat, mass and species transfer between phases represent the most important factors that influence the choice between those two operations. In this paper, both processes are discussed using computational CFD simulation through ANSYS-Fluent software. Only 3D half section of the packed column was considered with one packed bed. The packed bed was characterized in our case as a porous media. The simulations were carried out at transient state conditions. A multi-component gas and liquid mixture were used out in the two processes. We utilized the Euler-Lagrange approach in which the gas was treated as a continuum phase and the liquid as a group of dispersed particles. The heat and the mass transfer process was modeled using multi-component droplet evaporation approach. The results show that the counter-current process performs better than the co-current, although such limitations of our approach are noted. This comparison gives accurate results for computations times higher than 2 s, at different gas velocity and at packed bed porosity of 0.9.

Keywords—Co-current, counter current, Euler Lagrange model, heat transfer, mass transfer.

I. INTRODUCTION

DISTILLATION columns are considered as one of the reactor processes based on the separation of a mixture of gases to pure component by the evaporation and condensation. These columns are also known as biphasic reactors which operate with two fluid phases gas and liquid. LPG column allows the separation of pure hydrocarbons; ethane, methane, propane and n-butane from a multi-component liquid mixture [1]-[3]. This column consists of a vertical cylinder with two packed beds, two distributor plates of liquid phase and nozzles (Fig. 1). The gas spreads inside the column as a continuous phase while the liquid is introduced as a group of multi-component particles.

Two modes of contact between gas and liquid phase are studied; the co-current and the counter current mode [4], [5]. For the co-current process, the two fluids enter at one nozzle, flow through the column in the same direction and leave at the other nozzle. For the counter current process, the two fluids enter from different nozzles, flow in opposite direction and leave at different nozzles. The residence time, heat and mass transfer between phases are the major factors allowing determination of the kind of the contact.

Despite a rich literature dealing with packed bed reactors, there are only few works which presented the comparison between co-current and counter current process. Several studies [6], [7] modeled the heating and the evaporation of bi-component droplet in a hot air. They computed one single droplet in a 2D flow domain and they revealed the effect of the Reynolds number on the droplet evaporation rate. Shirodkar [8] took a cone spray for modeling and a urea water mixture for the drops. Nasr et al. [9] studied the heat and mass transfer of a binary film of water and ethylene glycol flowing in a vertical channel.

Seno et al. [10] experimentally observed the change in mass of water to the air within a counter current bubble column. For multi-component droplet, [11] explored the levitation technique to measure the heat transfer and the size of the drop during the evaporation of more than five components in the aqueous phase.

For the packed bed, [12] computed the simulation of liquid flow within the packed bed which is considered as an unstructured porous geometry. They used a combined volume of fluid VOF and Euler-Euler approach to determine the density of liquid.

The objectives of the present study were: (a) To compute the behavior of multi-component particles in two cases of co-current and the counter current flow and (b) To compare heat and mass transfer of the two modes of contact.

H. Troudi is with the Mechanical Laboratory of Sousse "LMS", Technopole BP264 Erriadh, 4023 Sousse, Tunisia (phone: +21624998098; e-mail: hajer.troudi@ gmail.com).

M. Ghiss, Phd. is with the Mechanical Engineering in Mechanical Laboratory of Sousse "LMS" (phone: +216 20909548; e-mail: moncefghiss@gmail.com).

Z. Tourki is Professor in Mechanical Engineering, National Engineering School of Sousse "ENISo", Mechanical Laboratory of Sousse "LMS", Technopole BP 264 Erriadh,4023 Sousse, Tunisia (phone: 00 216 73 369 500; fax: 00 216 73 369 506; e-mail: zbrtourki@gmail.com).

M. Ellejmi is General Manager in Alpha Engineering International, AEI. Sahloul III 4054, Sousse, Tunisia (phone: +21673821245/246/247; fax: +216 73821249; e-mail: m.ellejmi@alpha-engineering.com.tn).
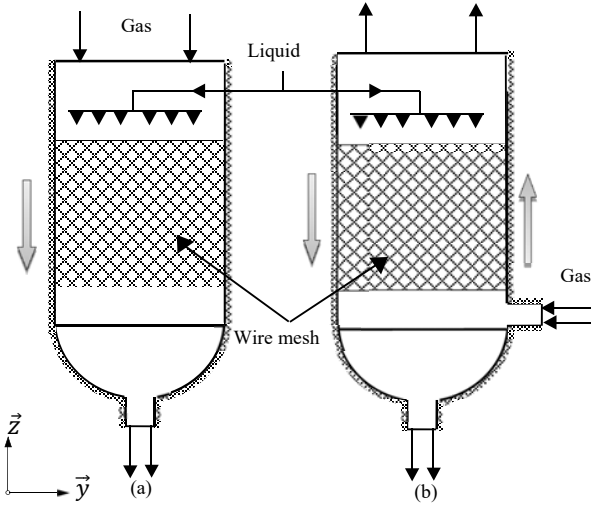
Fig. 1 Flow regimes in two-phase packed bed reactors: (a) Gas and liquid in co-current flow, (b) Gas and liquid in counter current flow

II. METHOD

Two approaches are used to model multiphase problems: The Euler-Euler and the Euler-Lagrange [13], [14]. In this work, the Lagrangian model was found much more appropriate for multi-component modeling than the Euler-Euler approach. The gas phase is used for the continuum phase and the discrete phase is considered as a group of particles of various species in the liquid phase. These particles are modeled as a spherical point and their positions, in the two processes, are spatially fixed. The appropriate governing equations involving three-dimensional transient state, laminar flow, and equilibrium multi-component vapor-liquid were employed in the design of two processes. The numerical methodology has been accomplished by the commercial software FLUENT 14.0.

In this section, we present equations of two phase flow as well as the mass and heat transport phenomena. In Euler-Lagrange model, the subscript q and p refers to the gas and the particle phases, respectively.

A. Continuous Phase

The gas phase was taken as the primary phase. The dynamics of this phase are computed by solving the Navier-Stokes equations in cylindrical coordinates. The mass, the momentum, the energy and the species conservation equations can be written as:

– Gas phase continuity equations:

$$\frac{\partial(\rho_q)}{\partial t} + \nabla\left(\rho_q \overrightarrow{V_q}\right) = S_m \tag{1}$$

– Gas phase momentum equation:

$$\frac{\partial\left(\rho_q \overrightarrow{V_q}\right)}{\partial t} + \nabla\left(\rho_q \overrightarrow{V_q}\overrightarrow{V}_q\right) = -\nabla p_q + \nabla\left(\overline{\overline{\tau_q}}\right) + \rho_q \vec{g} + \overrightarrow{F} \tag{2}$$

– Gas phase energy equation:

$$\frac{\partial(\rho_q E_q)}{\partial t} + \nabla\left(\overrightarrow{V_q}\left(\rho_q E_q + p\right)\right) = -\nabla\left(k_{eff}\nabla T - \sum_{i=1}^{N} h_q \overrightarrow{J_i} + \overline{\overline{\tau}}.\overrightarrow{V_q}\right) \tag{3}$$

– Gas phase species equation:

$$\frac{\partial(\rho_q Y_i)}{\partial t} + \nabla\left(\rho_q \overrightarrow{V_q}Y_i\right) = -\nabla\left(\overrightarrow{J_{i,q}}\right) \tag{4}$$

where ρ_q and V_q are the density, and the velocity of the continuous phase, respectively. p_q, τ_q and g represent the pressure, the viscosity stress and the gravity acceleration, respectively. S_m is the mass source added to the continuous phase from the dispersed second phase due to evaporation of liquid particles. This source is calculated from (13). F represents all the body forces due to interaction of the discrete phase with the continuous phase (6), as well as, the force of the porous media as described later in (7).

In (3), k_{eff}, $J_{i,q}$ and Y_i represent the effective conductivity, the diffusion flux and the mass fraction of species i in the gas mixture, respectively. The first three terms on the right-hand side of (3) represent energy transfer due to conduction, species diffusion and viscous dissipation. The term of species diffusion can be written by Fick's law [16] as:

$$\overrightarrow{J_{i,q}} = -\rho_q D_{i,m} \nabla Y_{i,q} - D_{T,i}\frac{\nabla T}{T} \tag{5}$$

where $D_{i,m}$ is the mass diffusion coefficient for species in the gas mixture, and $D_{T,i}$ is the thermal diffusion coefficient.

B. Dispersed Phase

The momentum equation for particles of density ρ_p dispersed into a carrier fluid of density ρ_q can be expressed in Lagrange frame as:

$$\frac{d\left(m_p \vec{V_p}\right)}{dt} = \vec{F}_{hy} + \vec{F}_P + \vec{F}_g + \vec{F}_D + \vec{F}_{lift} + \vec{F}_{vm} + \vec{F}_{ext} \tag{6}$$

where V_p is the velocity of each individual particle. The terms on the right-hand side represent the forces resulting from the interaction of particles with each other as well as with its surrounding gas. These forces are respectively, the drag force with C_D is the drag coefficient given by Morsi and Alexander [16]. This force defines the effects of turbulence Re of the gas stream on the particle drag coefficient C_D. The second term is the combined effects of buoyancy and gravitational force of the particle, and the third forces F_{ext} are forces due to added mass, pressure, lift, etc [16].

C. Porous Medium

The presence of packed bed within the column reduces the flow of the fluid through it, increases the residence time between phases to enhance heat and mass transfer, and causes rise to a pressure drop in the fluid. Using Ergun's law [15], [16],

the pressure drop across the length Δz of packed bed is defined as:

$$-\frac{\Delta P_{k,z}}{\Delta z} = 150\frac{\mu_k}{d_\Phi^2}\frac{(1-\Phi)^2}{\Phi^3}\vec{V}_k + 1.75\frac{\rho_k}{d_\Phi}\frac{(1-\Phi)}{\Phi^3}\vec{V}_k^2 \quad (7)$$

where Φ is the porosity that is characterized by the bed voidage and d_Φ is the diameter for spherical pores. The pressure loss is composed of two terms. The primary term is the viscous loss and the second is the inertial loss.

– Viscous resistance:

$$\frac{1}{K} = \frac{150}{d_\Phi^2}\frac{(1-\Phi)^2}{\Phi^3} \quad (8)$$

– Inertial resistance:

$$\frac{1}{C_2} = \frac{1.75}{d_\Phi}\frac{(1-\Phi)}{\Phi^3} \quad (9)$$

where K is the permeability of the packed bed and C_2 is the inertial loss coefficient. The momentum equation (2) can be written in the following form with addition of the source term of the porous media:

$$\frac{\partial(\rho_q\vec{V}_q)}{\partial t} + \nabla(\rho_q\vec{V}_q\vec{V}_q) = -\nabla p_q + \nabla(\overline{\overline{\tau}}_q) + \rho_q\vec{g} - \frac{\Delta P_{k,z}}{\Delta z} + \vec{F} \quad (10)$$

D. Equilibrium Vapor-Liquid

In each contact of the phases in porous medium, we assumed that the liquid phase and the gas phase are in equilibrium by Raoult's law [16]. The equations are as:

$$Y_i - K_i X_i = 0 \quad (11)$$

$$\sum_{i=1}^{N} Y_i = 1, \quad \sum_{i=1}^{N} X_i = 1 \quad (12)$$

where i is the particle type of species, Y_i is the vapor composition, X_i is the liquid composition of species i in the particle p and K_i is the value defined for each specie as the ratio.

E. Mass Transfer

The disperse and continuous phase are coupled by the relation of heat and mass transfer. The equation of mass transfer caused by conduction, convection and diffusion in the system is given as:

$$\dot{m}_p = \frac{dm_p}{dt} = \pi d_p \frac{\mu_q}{Sc_p}(2 + 0.6\,\mathrm{Re}_p^{1/2}\,Sc_p^{1/3})\ln\left(1 + \frac{Y_{p,s} - Y_{i,q}}{1 - Y_{p,s}}\right) \quad (13)$$

where m_p and d_p are the mass and the diameter of the particle, respectively. $Y_{p,s}$ is the vapor mass fraction at the surface of the particle and $Y_{i,q}$ is the vapor mass fraction in the bulk gas. In convection systems, the Reynolds number Re_p and the Schmidt number Sc_p characterize the dimensionless rate of mass transport at the surface of the particle.

F. Heat Transfer

The convection heat transfer is the summary of sensible heat and latent heat. The equation of heat transfer can be represented as:

$$m_p c_{p_p}\frac{dT_p}{dt} = h\pi d_p^2(T_q - T_p) + \sum_{i=1}^{N}\left(\frac{dm_p}{dt}(h_{vap})\right) \quad (14)$$

where c_p is the particle heat capacity. T_q and T_p are the temperature of continuous and dispersed phase, respectively. h is the convective coefficient and h_{vap} is the latent heat of vaporization.

III. SIMULATION DETAILS

Due to the column internals geometry and to the complex multi-component flow pattern inside it, also due to the axi-symmetric characteristic of the column, only the downer section with one packed bed and one distribution plate were explored for modeling (Fig. 1). Also, to reduce more the computational cost, Ansys Fluent can models packed bed as a porous material and describe it with a number of parameters.

The column dimension parameters are shown in Table I. The components of the liquid phase are shown in Table II. The position of each group of particles droplets are shown in Table III. The packed bed was modeled as a porous medium of porosity $\varepsilon = 0.9$ and length $l = 0.39$.

TABLE I
COLUMN PARAMETERS

Parameters	Unity	Data
Diameter, D	mm	304.8
Nozzle diameter, d_0	mm	0,01
Length Column, L	mm	0.6
Length packed bed, l	mm	0.3943648
Packing material	-	Raschig rings
Pore diameter, d_Φ	mm	0.015

TABLE II
LIQUID COMPOSITIONS DATA

Species	Molecular Formula	Mass Fraction
Methane (l)	CH_4	0.01163603
Ethane (l)	C_2H_6	0.930882
Propane (l)	C_3H_8	0.00023272
n-Butane (l)	C_4H_{10}	0.00023272
n-Pentane (l)	C_5H_{12}	0.015246
n-Hexane (l)	C_6H_{14}	0.00121145
Benzene (l)	C_6H_6	0.00325
n-Heptane (l)	C_7H_{16}	0.01125
Toluene (l)	C_7H_8	0.0111417
n-Octane (l)	C_8H_{18}	0.0012255
n-Decane(l)	$C_{10}H_{22}$	0.01369188

The walls are adiabatic. The pressure of the reference was assumed to be at 29 bar. The gas was taken as an ideal and compressible gas "Ethane". The laminar model was used in the simulation and the gravity was considered in this study.

Using ANSYS Fluent software, the geometry of the two models (Fig. 2) was developed as a three dimensional fluid model.

TABLE III
GROUP OF PARTICLES' POSITIONS

Number of group of particles	x (m)	y (m)	y (m)
1	0	0	0.33
2	-0.06	0	0.33
3	0.06	0	0.33
4	0	0.66	0.33
5	0	-0.66	0.33
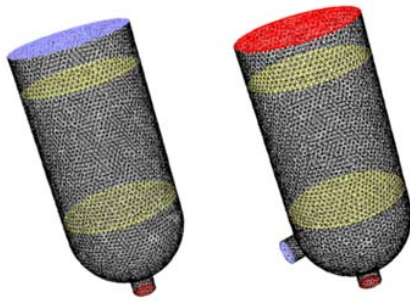
Fig. 2 CFD domain
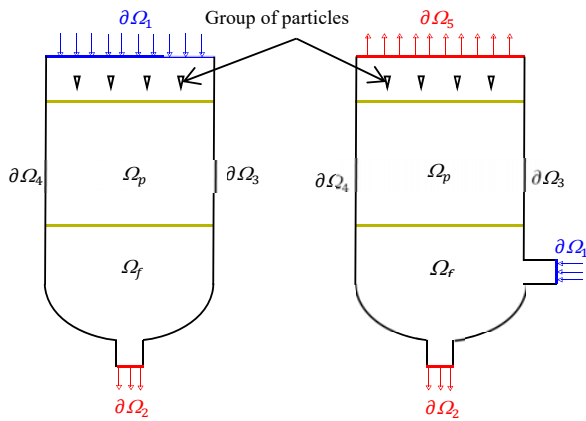
Fig. 3 Boundary conditions and computational domain for the numerical simulation

TABLE IV
BOUNDARY CONDITIONS

Boundary Condition Surfaces	Imposed Condition	Mass Flow	Temperature	Pressure
Surface $\partial\Omega_1$	Inlet	Q_q= 10 kg/h $Q_{p, Perfore}$= 2 kg/h	T_q= 121.8 °C $T_{p, Perfore}$= 33.36 °C	P_q= 0 bar P_p= 0 bar
Surface $\partial\Omega_2, \partial\Omega_5$	Outlet	Q_q= 0 kg/h $Q_{p, Perfore}$= 0 kg/h	T_q= 0 °C $T_{p, Perfore}$= 0 °C	P_q= 0 bar P_p= 0 bar
Surface $\partial\Omega_3, \partial\Omega_4$	wall	Q_q= 0 kg/h $Q_{p, Perfore}$= 0 kg/h	T_q= 0 °C $T_{p, Perfore}$= 0 °C	P_q= 0 bar P_p= 0 bar

For the comparison, we used the same boundary conditions for the two phases as shown in Fig. 3. There are two inlets and two outlets. The boundary condition realized to the inlet was taken the mass flow inlet. The outlet boundary condition was taken the pressure outlet. For both phases, the initial conditions used in the simulation are given in Table IV. Boundary conditions in porous zone of the simulations are presented in Table V. The viscous resistance and inertial resistance coefficients were calculated using (8) and (9).

TABLE V
BOUNDARY CONDITIONS FOR PACKED BED

Parameters	Unity	Data
Porosity, Φ	-	0.9
Viscous resistance coefficient, $1/K$	m^{-2}	8313.0156
Inertial resistance coefficient, $1/C_2$	m^{-1}	30.313

IV. RESULTS AND DISCUSSION

In this section, we have divided the results of our simulations into three parties.
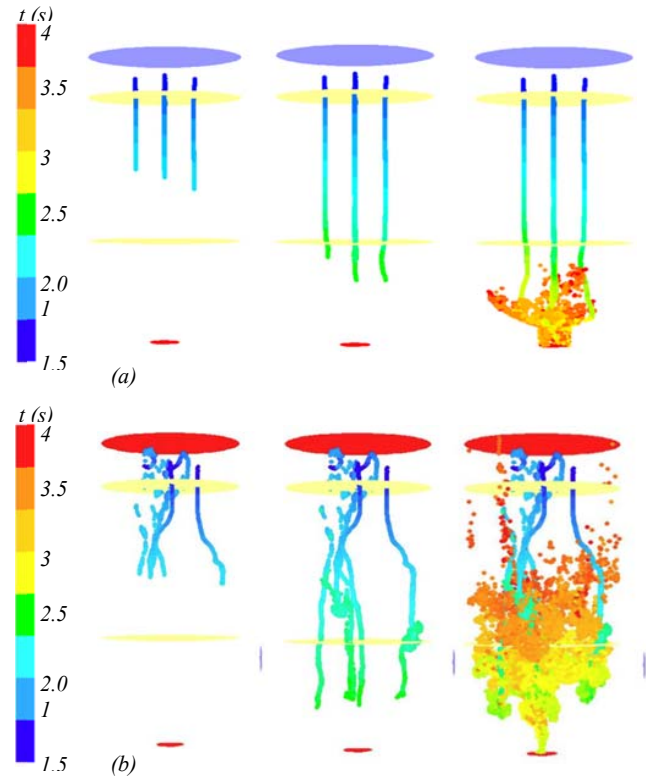
A. The Displacement of Particles

Fig. 4 Trajectory of particles colored by residence time in co-current and counter current process

Fig. 4 shows the trajectories of 10 μm evaporating multi-component particles inside the two cylinders in different times (1, 2 and 4 s). We can see the effect of gravity on the downward movement of particles and the influence of the gas phase over the two flow regimes (co-current and counter-current). In co-

current operation, Fig. 4 (a), the trajectory of liquid particles tends to be that of the velocity profile of the gas. The opposite effect is observed at a counter current. Fig. 4 (b) shows that the particles change their trajectories as they come close to the gas flow. Moreover, the mean residence time for the gas and liquid phase depends on the mode of operation. The time taken for the particles to slide down the outlet in counter-current operation is significantly higher than in co-current operation. This way, a sufficient contact between phases inside the column can guaranteed and one of the global objectives of the column design can reached.

B. The Particle Temperature
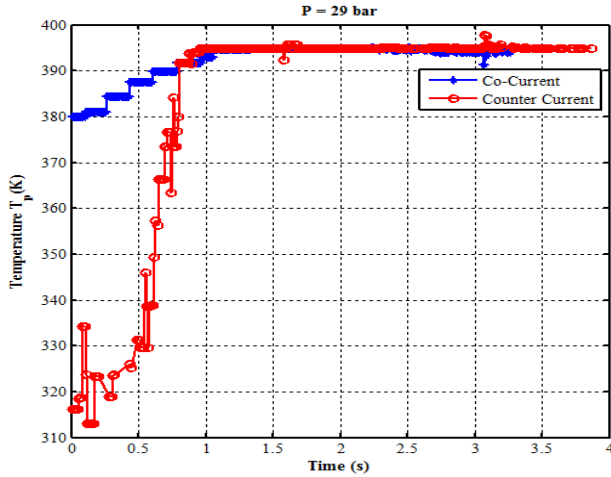
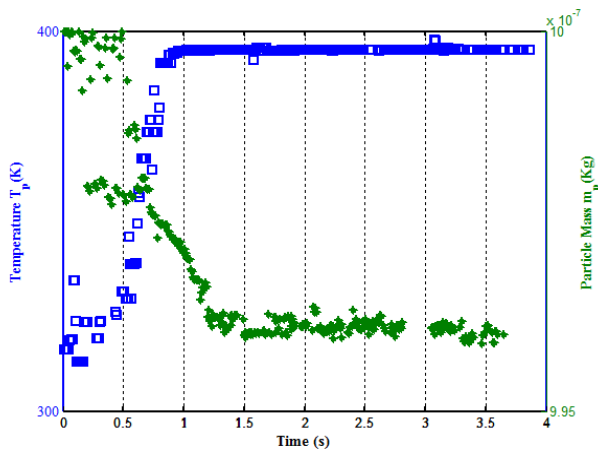Fig. 5 Particle temperature variation in both configurations with time

Fig. 6 Time evolution of particle mass (m_p) and surface temperatures (T_p)

Fig. 5 shows the plots of the particle's surface temperature T_p (K). At $0 \text{ s} \leq t \leq 1,6 \text{ s}$, the time-temperature profile of particles temperature sharply increases almost to the temperature of the gas phase "ethane". Due to the difference of temperature between phases, the gas phase heats the particles by thermal conduction and convection. During the heating, the thermal energy supplied by the gas initializes the evaporation on the surface of these particles and then contributes to the diffusion

and the migration of such species into the gas bulk. The equations for particles diffusion (4) are presented in Section II, as well as the heat and the mass transfer is computed respectively from (14) and (13). After $t \cong 1.6 \text{ s}$, the temperature is stable at 121.77 °C. The two phases reach their equilibrium temperature and the particles neither heat up nor cool down. The two phases are in thermal equilibrium.

In Fig. 6, we traced the evolution of the particle mass and the surface temperature with the time. As shown, the particle loses mass progressively when the temperature begins to rise. This reduce of mass promotes two effects: The breakup of the particle and the vaporization of species.

C. The Mass Fraction of Species

In this part, we have tracked the behavior of a single particle of one in five injectors and we have computed with the time the state of each species in the vapor Y_i and the liquid X_i phase respectively.
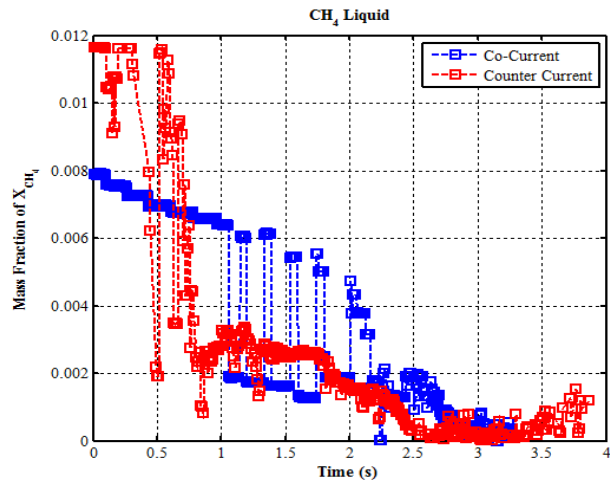

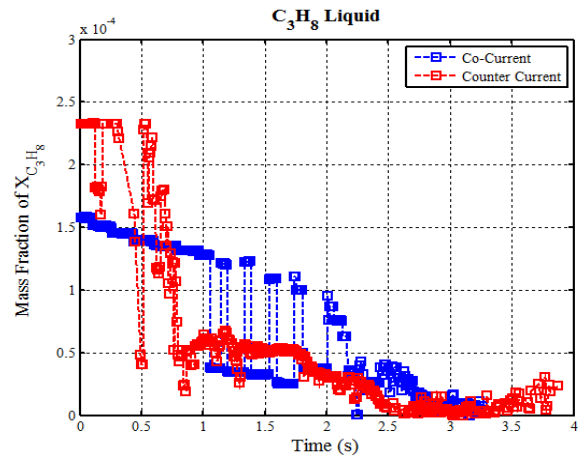Fig. 7 Liquid Mass fraction of CH_4 in co-current and counter current process

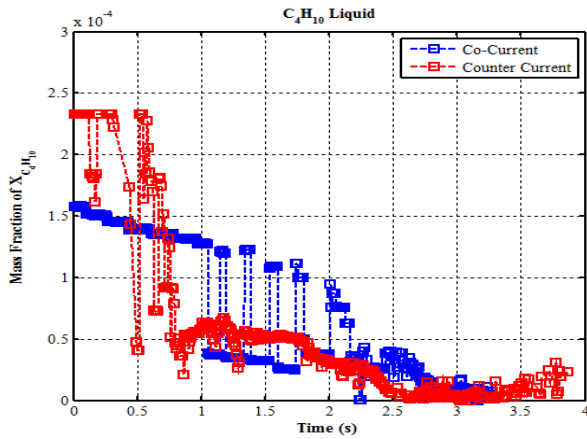Fig. 8 Liquid Mass fraction of C_3H_8 in co-current and counter current process

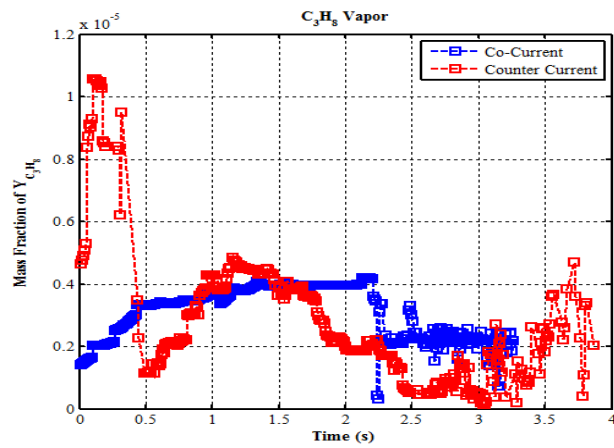Fig. 9 Liquid Mass fraction of C_4H_{10} in co-current and counter current process

Fig. 12 Vapor Mass fraction of C_3H_8 in co-current and counter current process
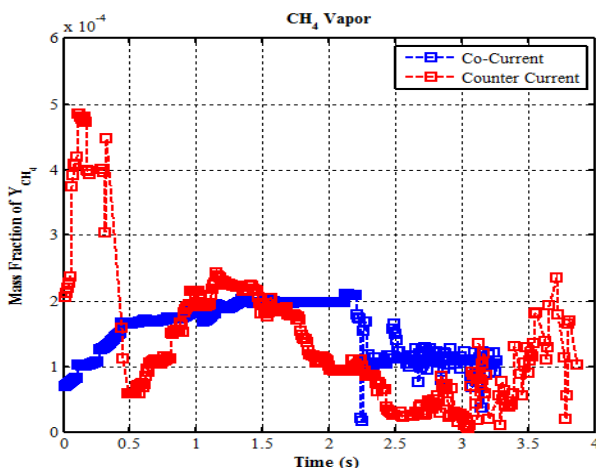

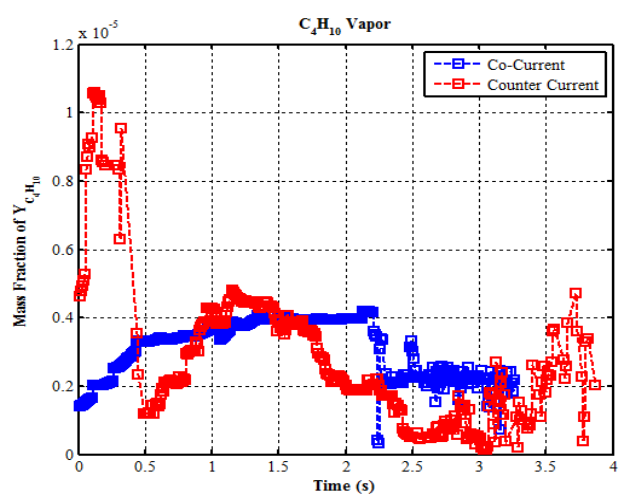Fig. 10 Vapor Mass fraction of CH_4 in co-current and counter current process

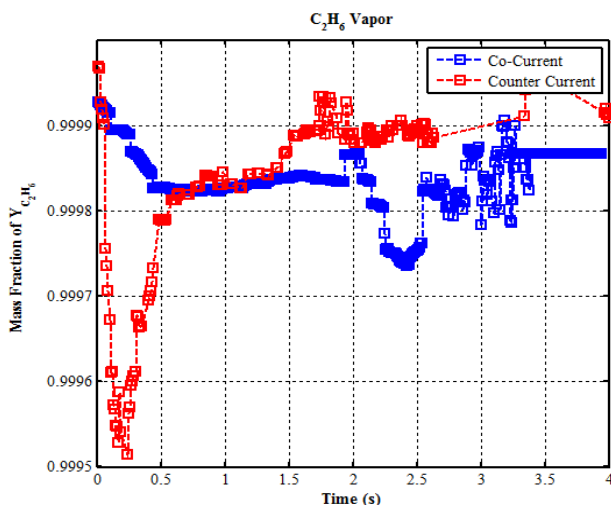Fig. 13 Vapor Mass fraction of C_4H_{10} in co-current and counter current process

Fig. 11 Vapor Mass fraction of C_2H_6 in co-current and counter current process

At t = 0 s, the column is full of C_2H_6 with mass fraction Y_{C2H6} = 1 (see Fig. 11). At t > 0 s, once the particles begin to inject into the continuous phase, the mass fraction of four primary species CH_4 (Fig. 7), C_3H_8 (Fig. 8), and C_4H_{10} (Fig. 9) in each particle decreases with time. On otherwise, we observed the appearance of those species in the vapor phase (Figs. 10, 12 and 13). This change of state is due to the diffusion of the most volatile species within the particle (4) and their evaporation (13) as mentioned earlier in the part *B*. the particle becomes increasingly rich in the less volatile species which are n-Pentane, n-Hexane, Benzene, n-Heptane, Toluene, n-Octane and n-Decane. As can be seen from the figures, CH_4, C_3H_8 as well as C_4H_{10} are quite similar. Their difference is in the value of the mass fraction. The species evaporate at different rates; the mass fraction of CH_4 is higher than C_3H_8 and C_4H_{10}. In the counter current, a significant drop in the mass fraction of species in the particle was occurred very rapidly than the co-current.

D. The Mass and Heat Transfer

This part is concerned with the mass and heat behavior in co-current and counter current process at different gas mass flow. The results obtained are shown in Tables VI and VII.

TABLE VI
MASS VS HEAT TRANSFER IN CO-CURRENT MODEL

Gas mass flow	Rate of mass transfer (Kg)	Rate of heat transfer (J)
2	0.0005455	3240
10	0.0014550	3240
15	0.0005593	1220
30	0.0007297	1810
50	0.0001477	2750

TABLE VII
MASS VS HEAT TRANSFER IN COUNTER CURRENT MODEL

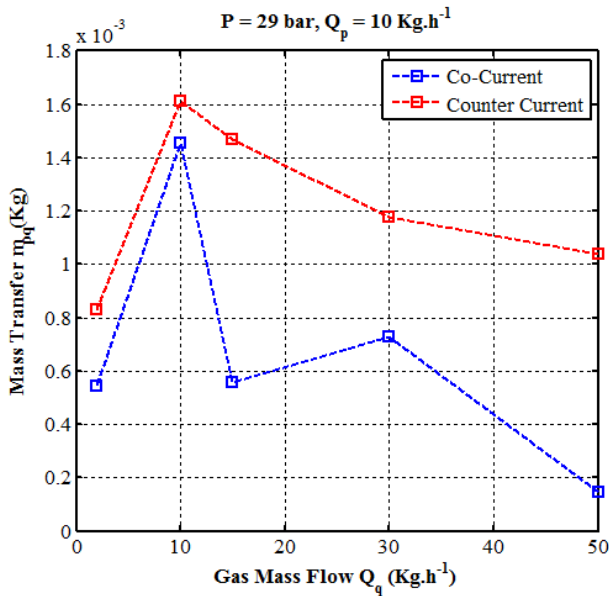| Gas mass flow	Rate of mass transfer (Kg)	Rate of heat transfer (J)
2	0.0008296	3522
10	0.0016120	3340
15	0.0014710	2780
30	0.0011790	2590
50	0.0010390	2430

Fig. 14 Variation of mass transfer in co-current and counter current process

As shown in Figs. 14, 15 and for a fixed particles mass flow $Q_p = 10$ Kg.h^{-1}, the increase of gas mass flow generates the decrease in both mass and heat transfer of co-current and counter current process. In this case, at high flow rates, the clogging phenomenon can occur. The particles flow is clogged by the moving of gas phase. The comparison of two co-current and counter current heat and mass transfer shows that the counter current flow mass transfer is higher than in case of co-current.
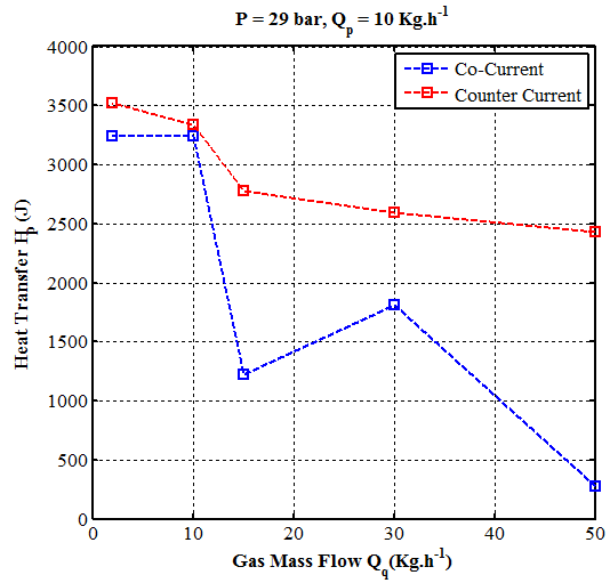

Fig. 15 Variation of heat transfer in co-current and counter-current process

V. CONCLUSION

In this work, we tried to solve a part of industrial problems. We compared the performance of co-current and counter current modes of operation in a LPG packed bed reactor. We used Ansys Fluent for modeling. The results obtained up to now show that the counter-current is more efficient than the co-current operation in terms of heat and mass transfer.

NOMENCLATURE

c_p	specific heat capacity of the material (kJ/kg.K)
d_Φ	pore diameter of packed bed (um)
d_p	particle diameter (um)
F	additional force (N)
F_D	drag force (N)
F_{vm}	virtual mass force (N)
F_{lift}	lift force (N)
F_{hyd}	hydraulic force (N)
F_g	gravitational force (N)
F_{ext}	exterior force (N)
Re	Reynolds number
h	convection heat transfer coefficient (kJ/m^2.s.K)
h_{vap}	latent heat of vaporization (kJ/m^2.s.K)
g	gravitational constant (g = 9.80665 m.s^{-2})
k	phase (q, p)
m	mass flow rate (Kg.h^{-1})
N	number of species
S	source term
Sc	Schimdt number
t	time (s)
T	temperature (K)
V	fluid velocity (m/s)
p	pressure (Pa)
X	mass fraction in liquid
x	mole fraction in liquid
Y	mass fraction in vapor
y	mole fraction in vapor
Z	mass fraction in feed

z mole fraction in feed

Greek Letters

α phase volume fraction
ρ density (kg.m^{-3})
μ dynamic viscosity (kg/m. s)
τ viscosity stress (Pa)

Subscripts and Superscripts

i specie
k phase
l liquid
m mixture
q continuous phase
s surface of the particle
p particle
v vapor
$*$ equilibrium condition

REFERENCES

[1] V. R. Dhole, B. Linnhoff, "Distillation column targets", *Computers Chemical Engineering*, vol. 17, n° 516, pp. 549-560, 1993.

[2] R W. Rousseau, Handbook of Separation Process Technology. Georgia Institute of Technology, 1987.

[3] M. Soos, E. Graczova, J. Markos, A. Molnar, P. Steltenpohl, "Design and simulation of a distillation column for separation of di-chloropropane from a multi-component mixture", *Chemical Engineering and Processing*, vol. 42, pp. 273-284, 2003.

[4] A. Ghareghashia, S. Ghadera, b, H. Hashemipoura, H. R. Moghadamc, "A comparison of co-current and counter-current modes for Fischer–Tropsch synthesis in two consecutive reactors of oxidative coupling of methane and Fischer–Tropsch", *Journal of Natural Gas Science and Engineering*, vol. 14, pp. 1-16, 2013.

[5] C.T. Blaisdell, K. Kammermeyer "Counter-current and co-current gas separation", *Chemical Engineering Science*, vol. 28, n° 6, 1973.

[6] R. Banerjee, R. Gopinath, "CFD Analysis to study evaporation of a single Ethanol / Iso- binary mixture droplet", *ASME-JSME-KSME 2011 Joint Fluids Engineering Conference*, July 2011.

[7] M. Vohra, "Evaporation of Ethanol / Iso-Octane Droplets (A Binary Component Fuel)", 2011.

[8] V. Shirodkar, "urea -water droplet phase change and reaction modelling: multi -component evaporation approach", *Frontiers in heat and mass transfer (FHMT)*, vol. 7, n° 5, 2016.

[9] A. Nasr, A. Belhadj Mohamed, J. Orfi, C. Debissi, S. Ben Nasrallah, "Evaporation of a thin binary liquid film covering one plate of a vertical Channel", *Revue des Energies Renouvelables*, vol. 11, n°4, pp. 611 – 622, 2008.

[10] T. Seno, S. Uchida, S. Tsuyutani, "Mass transfer in counter current and cocurrent bubble columns", *Chemical Engineering Technology*, vol. 13, n° 1, pp. 113–118, 1990.

[11] J. F. Widmann, E. J. Davis, "Evaporation of Multicomponent Droplets", *Aerosol Science and Technology*, vol. 27, n° 2, pp. 243-254, 1997.

[12] P. Niegodajew, D. Asendrych, M. Marek and S. Drobniak, "Modelling liquid redistribution in a packed bed", *Journal of Physics,* vol. 530, 2014.

[13] M.J.V. Goldschmidt, B.P.B. Hoomans, J.A.M. Kuipers, "Detailed comparison of Euler-Lagrange and Euler-Euler models for simulation of dense gas fluidised beds*", 10th Workshop on Two-phase Flow Predictions*, pp. 285-299, April 2002.

[14] Z. Zhang, Q. Chen, "Comparison of the Eulerian and Lagrangian methods for predicting particle transport in enclosed spaces" *Atmospheric environment*, vol. 41, n° 25, pp. 5236-5248, August 2007.

[15] J.-P. Wauquier, "Tome 1: Pétrole brut, Produits pétroliers, Schéma de fabrication," Le raffinage du pétrole, p. 255, 1994.

[16] "Ansys fluent 12.0: Theory Guide," 2009.